# Diffraction-Limited Photogeneration and Characterization of Silver Nanoparticles

**Oliver L. A. Monti, John T. Fourkas,† and David J. Nesbitt***

*JILA, University of Colorado and National Institute of Standards and Technology, Boulder, Colorado 80309-0440*

*Received: April 22, 2003; In Final Form: August 1, 2003*

Visible-light-induced photogeneration of silver nanoparticles in a diffraction-limited focal region is demonstrated. The photochemical growth depends quadratically on illumination intensity indicative of a multiphoton generation process, with the identity of the silver nanoparticles confirmed by UV/vis absorption spectroscopy. Mie simulations of the absorption spectrum reveal a size distribution dominated by Ag particles with radii in the range of a few nanometers. Spectrally resolved laser excitation and emission studies demonstrate that the likely luminescence source is surface-enhanced Raman scattering from silver nanoparticles, with spectral jumps occurring on a time scale comparable to that of fluctuations in the total luminescence intensity. Possible routes for the photogeneration process as well as identity of the Raman-active species are discussed. Such diffraction-limited photoproduction methods for luminescent silver nanoparticles offer novel routes toward optical data storage and nanometer-scale molecular sensing.

## I. Introduction

Considerable effort has been invested over the past decade in detailed investigations of optical and electronic properties of nanoscopic semiconductor and metal clusters and particles.[1−4] Advances in size- and shape-selective synthetic methods of simple or composite nanoparticles[5] have facilitated rapid progress in our understanding of the physics of nanomaterials, the boundary between molecular and solid-state physics. Silver nanoparticles have provided a particularly rich and ongoing focus of intense research efforts. This is in large measure due to their ability to sustain resonant collective electron oscillations, i.e., surface plasmons,[6] that can be optically excited in the near-ultraviolet or visible range of the electromagnetic spectrum, conveniently accessible with laser light sources. The spectral properties of the surface plasmon resonance are critically dependent on the shape, size, and spatial arrangement of the particles.[7] Tailoring these properties offers exciting prospects in fields from nanooptics[3] to biophysics.[8]

Observation of size-dependent physical properties in nanoparticles affords a unique opportunity to study the evolution from small-molecule to bulk-system characteristics. A particularly intriguing example is given by the fluorescence of noble metals. It is well-known that the quantum yield for fluorescence from smooth noble metal films is extremely small, on the order of $10^{-10}$ (see ref 9), where the fluorescence mechanism is thought to be radiative recombination of sp-conduction-band electrons with d-band holes.[9,10] The weak luminescence may be enhanced by approximately 1−2 orders of magnitude[11] on rough metal films and, as shown by El-Sayed and co-workers, dramatically by a factor of up to 1 million in gold nanorods.[12] This process was explained by plasmon enhancement of the interband transitions. Similarly, large fluorescence enhancement has been observed for 5 nm spherical gold nanoclusters, but not for larger nanoparticles.[13] At even smaller sizes, the surface plasmon band is largely absent.[14,15] Intriguingly, Dickson et al. reported recently on minute silver particles showing a structured luminescence band,[15,16] thus exhibiting properties characteristic of distinct molecular clusters. Studies in this area are complicated by the difficulty of generating and stabilizing very small clusters. Encapsulation in dendrimers,[15,17] stabilization by thiol ligands[18,19] as well as peptide-capping agents,[14] and embedding in glass matrixes[20] have shown some initial success in this direction. These reports provide important first insights into the size-dependent transition between molecule-like clusters and metallic nanoparticles. However, much work is still needed to characterize the evolution of bulk properties from their molecular or atomic origins.

For larger nanoparticles, it is the surface plasmon itself that gives rise to a number of interesting phenomena, in particular surface-enhanced Raman spectroscopy (SERS)[21] of surface-adsorbed molecules. Quantitative elucidation of the enhancement mechanism[22,23] and extension of ensemble-averaged SERS to the single-molecule limit[24] have received considerable attention in the recent literature. The detailed information available from vibrational spectra on a single-molecule basis has tremendous potential for physics and analytical chemistry on a nanometer scale. Most SERS work is performed either on rough silver films[25] or with molecules adsorbed on colloidal silver particles.[26] Despite a wealth of information available from SERS on such samples, there is a clear need for alternative sample preparations. Novel synthetic methods have the potential to shed light on some of the persistent questions and challenging problems in this field. First steps in this direction can be seen in a number of recent reports on in situ photoreduction of silver ions on silica nanoparticles at 514.5 nm to generate SERS-active samples,[27] as well as laser-induced coating of polystyrene spheres with silver particles.[28] Wu et al. demonstrated the feasibility of two-photon exposure of photographic films[29] and developed an 800 nm two-photon active photographic material based on a $AgNO_3$ solution in a wet $SiO_2$ gel matrix.[30] Perry and co-workers demonstrated two-photon laser writing of free-standing three-dimensional metal nanostructures in a composite material

* To whom correspondence should be addressed. Phone: (303) 492-8857. Fax: (303) 492-5235. E-mail: djn@jila.colorado.edu.

† Permanent address: Eugene F. Merkert Chemistry Center, Boston College, Chestnut Hill, MA 02467.

10.1021/jp030492c 
Published on Web 01/08/2004

consisting of $AgBF_4$, ligand-coated silver nanoparticles as seeds, a host polymer, and a sensitizing dye.[31] Slow growth of small nanoparticles upon illumination at 514 nm was observed also in the absence of the nanoparticle seeds. Particularly interesting in this context are recent efforts on photoactivated fluorescent silver clusters formed from silver oxide films[16,32] and silver salts in solution.[15,33]

Here we present experimental evidence for visible-light-induced photogeneration of silver nanoparticles in thin polymer films. We describe a method for creating strongly luminescent, diffraction-limited clusters of small, stable silver nanoparticles using a conventional confocal microscope setup. The strong luminescence can be attributed in part to a surface-enhanced Raman scattering process from molecules on the surface of the silver particles. We find a nonlinear dependence on illumination intensity for the growth kinetics, indicating a multiphoton process responsible for the photogeneration. We discuss possible origins for the time-dependent nature of the spectra and speculate on the mechanism for photoreduction and agglomeration to form the silver particles.

The paper is organized as follows: Section II describes the experimental procedures and apparatus used. Section III presents evidence of photogeneration of silver particles and discusses the nature of the strong observed luminescence. Section IV discusses the nature of the photogenerated silver particles. On the basis of Mie theory, we determine an approximate distribution of silver particle sizes (modeled as spheres) generated in the laser focus. Concluding comments are summarized in section V.

## II. Experiment

Silver perchlorate (99.9%), silver nitrate (99.9999%), polystyrene (polystyrene standard, molar mass 18700 g/mol), poly(methyl methacrylate) (PMMA; average molecular mass 15000 g/mol), toluene (spectranal grade, >99.9% purity), chloroform (spectrophotometric grade, >99.9% purity), and ethanol (spectrophotometric grade) are used as received without further purification. Samples are prepared by making a 10 mM solution of silver perchlorate in toluene with 1 mg of polystyrene per 1 mL of toluene or alternatively a 10 mM solution of silver nitrate in a mixture of chloroform and ethanol (1:1) with 1 mg of PMMA per 1 mL of solvent. A 50 $\mu$L sample of either solution is spin-coated directly onto an ozone-cleaned glass microscope coverslip. All experiments are conducted in air.

The optical setup consists of a conventional upright microscope equipped with a dry objective (100×, 0.90 NA). Excitation is provided by an argon ion laser (air-cooled, 488 nm), a doubled 1064 nm Nd:$YVO_4$ laser (532 nm), or a green helium−neon (HeNe) laser (543.5 nm), each coupled into a single-mode optical fiber for spatial filtering. The laser beam is expanded to slightly overfill the back aperture of the objective and passed through a narrow band-pass filter to eliminate weaker spectral lines emitted by the laser source, as well as fluorescence from optics prior to the microscope. The excitation beam is reflected off a dichroic beam splitter, designed to reflect excitation light and transmit red-shifted luminescence, and brought to a nearly diffraction-limited spot (full width at half-maximum $\Gamma_{fwhm} \approx$ 350 nm). The luminescence from the silver particles is collected by the same objective in epifluorescence geometry. Residual excitation light is suppressed using a combination of two interference filters (each of optical density >6), and the luminescence is focused onto the aperture of a multimode fiber (100 $\mu$m core diameter) acting as a confocal pinhole. In the imaging mode, the fiber is directly coupled to a single-photon-counting avalanche photodiode with dark count levels of approximately 90 counts per second (cps).

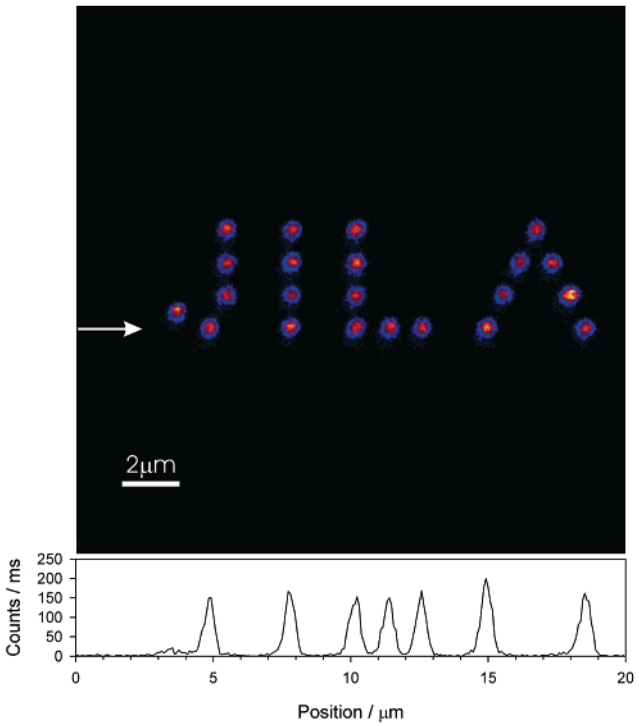


**Figure 1.** Image of photogenerated, diffraction-limited luminescent silver nanoparticles. The sample consists of 10 mM $AgClO_4$ in toluene with polystyrene (1 mg/mL), spin-cast in a thin film onto a glass coverslip. Each spot is generated at 488 nm illuminated at an intensity of 50 kW/cm$^2$ for 3 s. The image is acquired at 488 nm with an intensity of 0.5 kW/cm$^2$ and a dwell time of 1 ms per pixel. Image size: 20 $\mu$m by 20 $\mu$m. The trace at the bottom of the image shows a lineout taken at the position indicated by the arrow.

Data are collected in two modes of operation. In the imaging mode, a two-dimensional image (256 pixels by 256 pixels) of the sample is created by raster-scanning the sample on a computer-controlled three-axis closed-loop piezoelectric flexure stage. The silver particles are photochemically generated at arbitrarily chosen points on the sample and illuminated with intensities in the range of 0.4−60 kW/cm$^2$. To facilitate retrieval of previously generated silver particles when the excitation color is changed, an indexed grid (100 $\mu$m spacing) has been photolithographically imprinted onto the microscope coverslips. In the spectroscopy mode, the light from the multimode fiber is coupled into a Czerny−Turner-type spectrometer (grating 600 lines per mm, $f = 4$) and spectrally dispersed onto a liquid-nitrogen-cooled CCD detector. Spectra are typically accumulated for 4 s with a spectral resolution of approximately 10 cm$^{-1}$. Absorption spectra are measured using a standard UV/vis spectrometer.

## III. Results

We first present a sample image recorded after photogenerating luminescent species in the $AgClO_4$/polystyrene film. Figure 1 shows a 20 $\mu$m × 20 $\mu$m region with a regular array of photogenerated, diffraction-limited luminescent features. Each individual feature is generated by illumination for approximately 3 s at an intensity of 50 kW/cm$^2$ at 488 nm. After the desired pattern is written, an image is acquired at 488 nm with a low excitation intensity of 0.5 kW/cm$^2$ and a dwell time of 1 ms/pixel. The features are spatially confined to the area of the laser focal spot during writing and display an average contrast ratio

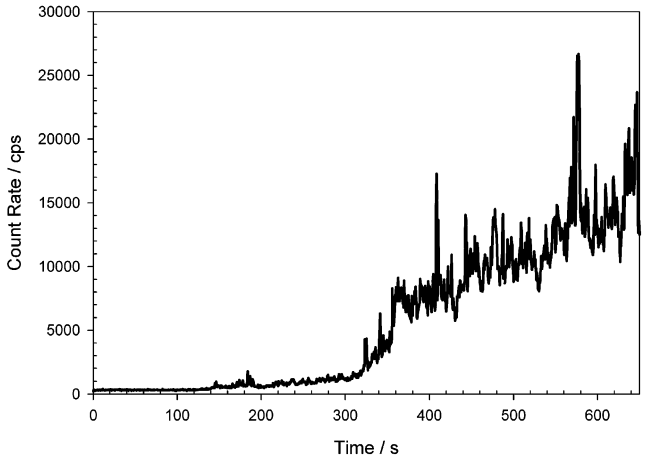


**Figure 2.** Time-dependent luminescence trace, recorded at 532 nm and an intensity of 0.5 kW/cm$^2$. The integration time per bin is 500 ms. The sample consists of $AgClO_4$ in polystyrene, spin-cast onto a glass coverslip.

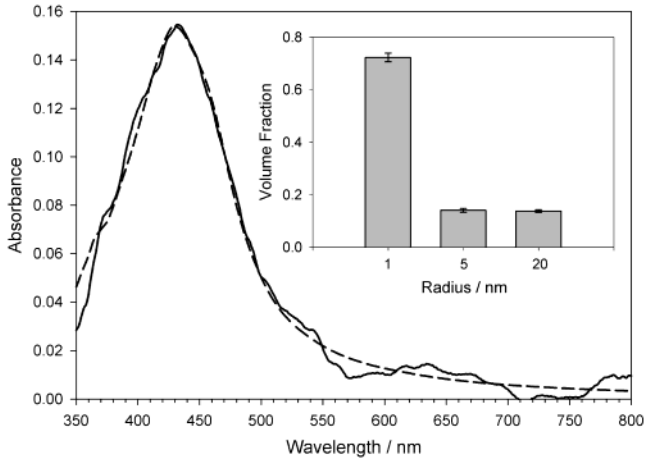


**Figure 3.** Solid line: UV/vis absorption spectrum of five coverslips, coated on both sides with a thin film of $AgClO_4$/polystyrene and illuminated for 10.5 h at 1.9 W/cm$^2$ and 532 nm. Dashed line: Simulation of the absorption spectrum based on modified Mie theory for a mixture of silver spheres with radii 1, 5, and 20 nm. A superposition of calculated surface plasmon spectra is a least-squares fit to the experimental spectrum. Inset: Size distribution of silver spheres obtained from a least-squares fit, displayed as volume fraction.

of 176(36):1. Similar images are recorded at all three laser wavelengths used in the present set of experiments. Intense illumination of silver perchlorate embedded in a polymer matrix thus leads to *localized* generation of a luminescent species.

A first indication of the nature of the luminescent species may be obtained by investigating the time dependence of the luminescence. Figure 2 shows a luminescence trace detected by illuminating a nearly diffraction-limited spot of $AgClO_4$ embedded in a thin polystyrene film on a glass coverslip. The sample is illuminated at 532 nm and at an intensity of 0.5 kW/cm$^2$, with each data point integrated for 500 ms. Under these conditions, we observe strong luminescence growth on the time scale of minutes, interspersed with large photon bursts, in some instances almost tripling the count rate. In Figure 2, the burst length varies between 500 ms, as limited by the integration time, and tens of seconds. It is important to emphasize that while the exact time-dependent luminescence pattern is different for each location on the sample, the strong time-dependent growth in luminescence, with large fluctuations superimposed, is observed at all positions on the sample and for all illumination wavelengths used. Furthermore, when the spin-coated samples are kept in the dark for periods of up to 6 h prior to laser excitation, no luminescent species can be detected immediately upon illumination. Growth of the luminescent species is thus clearly visible-light-induced and sustained throughout the illumination period of tens of minutes, suggesting the continuous generation of luminescent centers within the focal spot.

Identification of the luminescent species is achieved by recording an absorption spectrum after illumination of the thin film. A stack of five glass coverslips, spin-coated on both sides with a $AgClO_4$/polystyrene film, is illuminated with a 6 W 532 nm laser. The laser beam is expanded to a 1/e electric field diameter of 1 cm, and the sample stack is illuminated for 10.5 h. Under these conditions, the total number of photons impinging on the sample is comparable to that in the confocal microscopy setup, albeit at much lower average intensity. Figure 3 shows the absorption spectrum from this sample. We observe a broad ($\Gamma_{fwhm} \approx 100$ nm), strong band (peak absorbance 0.16) centered at 432 nm as well as a second, weaker band (absorption maximum 0.015 at 635 nm). The band in the blue end of the visible spectrum is characteristic of the Ag metal surface plasmon band, which for silver particles in a vacuum is found at 350 nm (see ref 6). In general, however, the position, width, and shape of the surface plasmon band are highly dependent on the size, shape, and environment of the particles[6,23] thus potentially red-shifting well into the visible spectrum. Figure 3 provides clear evidence for the visible-light-induced photogeneration of silver nanoparticles in the thin polymer film, at even lower intensities than used for recording the image in Figure 1. This suggests that similar photochemical processes take place in the focal spot of the microscope objective, and further confirms that silver nanoparticles are generated in a nearly diffraction-limited region.

The nature of the observed photoluminescence is first investigated by power-dependence studies. As shown in panel A of Figure 4, the luminescence scales linearly [slope $m =$ 1.014(25)] with illumination intensity over 2 orders of magnitude, clearly indicating a one-photon excitation of the luminescent species. Studies characterizing the formation process prove somewhat more challenging. Specifically, panel B of Figure 4 shows the total luminescence rate after 30 s of illumination at a series of excitation intensities, for which strong time-dependent fluctuations in the luminescence give rise to rather large scatter in this data set. However, the light-dependent kinetics clearly follow a process of approximately third order [slope $m =$ 3.25(47)] over the range of laser power investigated. In conjunction with the previously established linear dependence of the luminescence rate on excitation intensity, this therefore suggests an approximately quadratic intensity dependence for photogeneration.

Luminescence from photogenerated silver particles in the focal volume of the confocal microscope may result from either fluorescence from minute silver clusters[15,16,32−37] or emission of Raman-shifted photons. The latter process could be greatly enhanced by the presence of silver metal surfaces.[21] It is possible to distinguish these two processes spectroscopically. To achieve this, we collect spectra of luminescent photogenerated silver particles from single, nearly diffraction-limited spots and choose to represent them as a function of frequency shift with respect to the excitation wavelength. A representative series of spectra acquired over 80 s in the spectral range of 0−3000 cm$^{-1}$ is shown in Figure 5. The excitation wavelength is 488 nm, and the spectra are shown uncorrected for filter transmission. Similar data were acquired at all three excitation wavelengths available. Notice that the dominant feature in *all* spectra is a combination

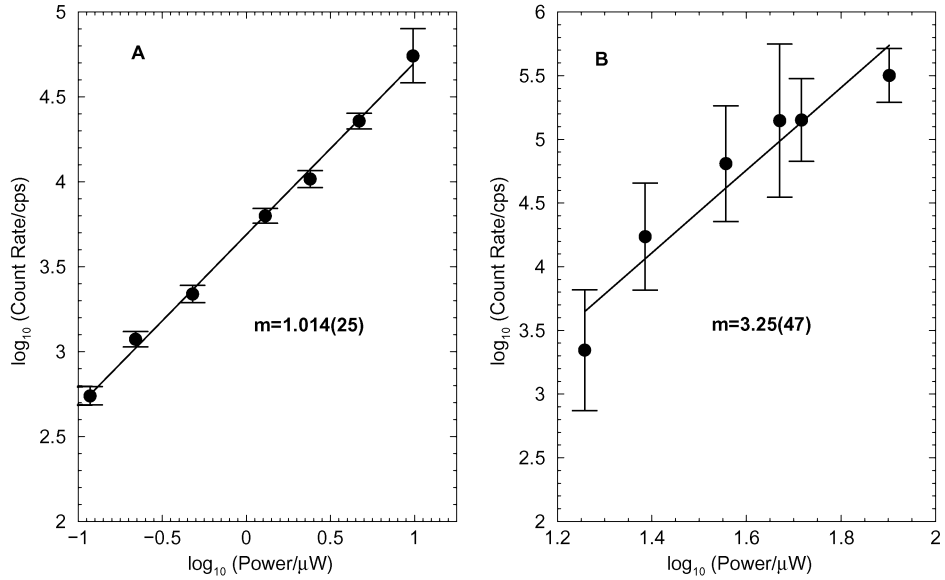


**Figure 4.** (A) Dependence of the luminescence rate as a function of intensity in the focal spot. (B) Dependence of the growth rate as a function of illumination intensity. The growth rate is determined by measuring the luminescence after 30 s of illumination. Sample: 10 mM $AgClO_4$ in toluene with 1% polystyrene, spin-cast onto a glass coverslip. Illumination wavelength: 532 nm.

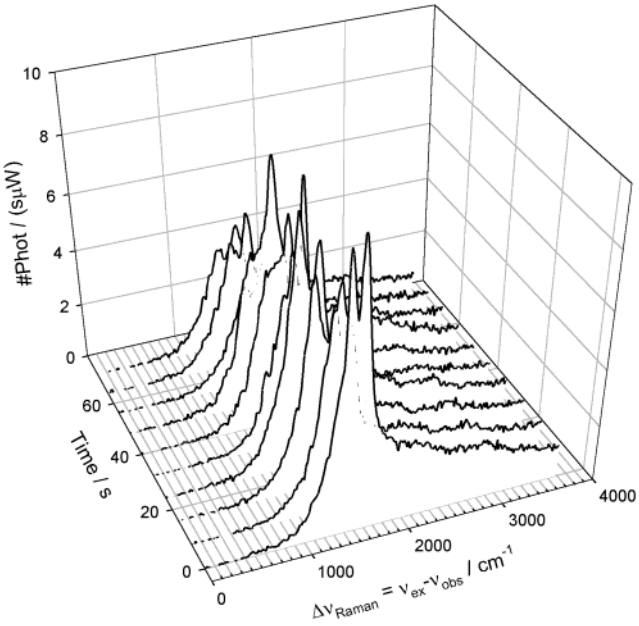


**Figure 5.** Spectral jumps of 488 nm excited luminescence in a sample spin-cast out of a $AgClO_4$/toluene/polystyrene solution. The integration time per spectrum is 4 s, intensity 50 kW/cm$^2$. The spectra are background-subtracted but not corrected for filter transmission. The spectra are shown as a function of the frequency shift from the excitation wavelength.

of bands in the range of 800−1800 cm$^{-1}$, with a strong intensity drop-off at large frequency shifts. The spectra also display remarkable spectral jumps, in both overall intensity and relative strength of the various spectral features within the characteristic structure. These fluctuations occur on a time scale comparable to that of the luminescence bursts observed in Figure 2, and therefore plausibly arise from a common origin.

The laser powers are relatively modest (500 nW to 75 $\mu$W), even for a diffraction-limited focus; the luminescence fluctuations and spectral jumps cannot be explained by heating-induced fusion and structural changes among multiple particles. Specifically, given the bulk heat capacity of silver of $C_p^{Ag}(300\ K) = 0.236$ kJ/(kg·K) and a bulk density of silver of $\rho_{Ag} = 10500$ kg/m$^3$, one can estimate an initial temperature rise of $\Delta T = 35$ K for the absorption of a single 500 nm photon by a 1 nm radius silver sphere. At the highest intensities employed (75 $\mu$W, $6 \times 10^4$ W/cm$^2$), the mean time between absorption events is approximately 2 ns ($\sigma_{abs} = 3 \times 10^{-15}$ cm$^2$ at 500 nm for a 1 nm radius silver sphere). Assuming heat transport over one silver particle diameter with a polystyrene bulk thermal conductivity of 0.187 W/(K·m),[38] the heat flow takes place on a time scale of approximately 30 ps, consistent with recent work by Hartland and co-workers.[39,40] This is considerably faster than the average time between absorbed photons even at the highest intensities used. CW-laser-induced melting of the silver nanoparticles is thus unlikely, and the spectral jumps must be considered together with the nature of the observed luminescence. Furthermore, the spectra in Figure 5 are recorded in a regime of saturated growth, i.e., where no additional increase in average intensity is observed with time. Photogeneration alone can thus be ruled out as a source of the spectral fluctuations.

Conclusive evidence of the emission source can be obtained by comparing luminescence spectra collected for three different photogeneration and excitation wavelengths. $AgClO_4$/polystyrene samples are illuminated at 488, 532, and 543 nm. Figure 6 shows three representative spectral snapshots as a function of the frequency shift with respect to the excitation frequency. Each panel shows both the raw, background-subtracted spectrum and the spectrum corrected for wavelength-dependent filter transmission. Notice that both generation and probing of the luminescent particles are performed at the same wavelength in each case. Above 2000 cm$^{-1}$, all spectra display diffuse and largely structureless luminescence. However, at each excitation wavelength, the spectra show the same characteristic broad superposition of bands in the range of 800−1700 cm$^{-1}$, with a relatively sharp edge at the large frequency shift end of the spectrum. The substructure in this main feature varies, as is expected on the basis of the spectral jumps shown in Figure 5 and observed at each individual excitation wavelength. We attribute the difference in fine structure to the time-dependent nature of the observed spectra, but emphasize the similarity of all three spectra. The relative contribution of these bands, $\Delta\tilde{\nu}_{Raman} \leq 1900$ cm$^{-1}$, to the spectrally integrated luminescence is 27% at 488 nm, 65% at 532 nm, and 58% at 543 nm as

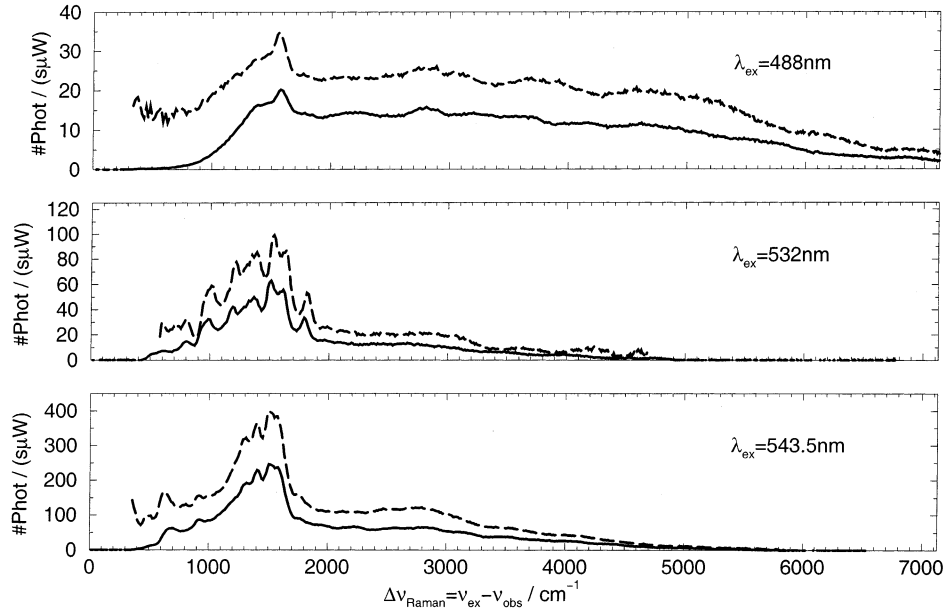


**Figure 6.** Luminescence spectra of diffraction-limited silver nanoparticle collection at three different wavelengths: 488 nm (top), 532 nm (middle), and 543.5 nm (bottom). Each spectrum represents a luminescent feature photogenerated and excited at the specified wavelength. Solid line: spectra are background-subtracted only. Dashed line: spectra are background-subtracted and corrected for wavelength-dependent filter transmission.

calculated from the filter-corrected spectra shown in Figure 6. From these data it must be concluded that the dominant part of this strong luminescence is due to a Raman process; it cannot be explained purely by fluorescence.

This result is at first quite surprising: Raman cross-sections[24] are typically prohibitively small ($\sigma_{\text{Raman}} \approx 10^{-30}$ cm$^2$) and do not allow for detection of a relatively small number of scatterers as might be found in the focal volume under the present experimental conditions. However, when a molecule is adsorbed onto a rough noble metal surface[21] or the surface of a small noble metal particle,[41] the optically excited collective surface electron motion strongly enhances the local electric field. Under these conditions, even single molecules can be detected by this surface-enhanced Raman process.[24] Due to the weak nature of the process we expect to detect such spectra of Figure 6 only for silver metal particles in close proximity to the Raman-active species. We thus interpret Figure 6 in conjunction with the absorption spectrum of Figure 3 as evidence for the localized photogeneration of silver nanoparticles, giving rise to surface-enhanced Raman scattering of molecules near or on the particle surface. This conclusion is further supported by experiments using different photogeneration and excitation lasers; irrespective of the photogeneration light source, the spectra yield structured Raman bands shifted consistently with respect to each laser excitation frequency.

## IV. Discussion

**IV.1. Photogeneration Mechanism.** Silver clusters play a crucial role in photography. While some aspects of the photographic mechanism remain to be elucidated, photoreduction of silver halide salts is known to produce small silver particles on the halide crystal surfaces.[37,42] The critical role of silver cluster formation in the photographic process and a desire to control photoinduced nanoparticle growth in general necessitate a better understanding of the sequence of chemical reactions involved in the photoreduction. There have been brief reports of visible-light-induced photogeneration of silver nanoparticles from silver salts by several groups. Muniz-Miranda describes a procedure to reduce silver ions onto a suspension of silica nanoparticles by irradiation at 514.5 nm in the presence of silver nitrate.[27] Crawford et al. have utilized the laser-induced generation of silver clusters on the surface of silver nitrate impregnated polystyrene particles.[28] To date, however, there have been no detailed studies of the mechanism for generating such SERS-active species. From our experiments, conducted in thin solid films, it is clear that neither the precursor salt nor the exact environment plays a crucial role in the formation of the silver particles. We observe photogeneration on bare glass surfaces, in various polymer films spin-cast from different solvents, and by illuminating silver perchlorate as well as silver nitrate. The photochemistry must thus proceed via a route independent of these parameters. The nonlinear intensity dependence of the photogeneration process indicates a two-photon reaction sequence, possibly involving excitation of multiple species to generate neutral silver atoms and clusters.

Dickson et al.[16] reported recently on the formation of minute *fluorescent* silver particles by illuminating silver oxide films ($\lambda < 520$ nm). Although no data are currently available on SERS from such particles, their work may shed light on a possible mechanism for the photoinduced formation of silver nanoparticles in our samples. The authors observed a photoactivation process where fluorescence could be excited at a range of wavelengths once the particles were photochemically generated. In contrast to our particles, the clusters thus formed may contain fewer than 10 silver atoms.[15,16] The mechanism for photoactivation is postulated to be initiated by absorption of a visible photon by $Ag_2O$, a semiconductor material with a band gap of 2.25 eV.[43] Photoexcitation of $Ag_2O$ is known to produce silver peroxide, AgO,[44] which may photolytically form $Ag^0$. Further evidence for this mechanism was obtained from the photoactivated generation of fluorescent silver particles from AgO films.[32] Such a light-induced reaction sequence may thus supply a nucleation site for the growth of silver clusters in our system, provided the presence of silver oxide or silver peroxide. This mechanism, supported by the intensity dependence of the photogeneration step, hinges critically on the presence of atmospheric oxygen and silver oxides in the sample; investigations under vacuum and in oxygen-enriched environments are

thus currently under way. It will be particularly interesting to test the role of $Ag_2O$ as an intermediate species by illumination at wavelengths longer than 550 nm, i.e., below the band gap of silver(I) oxide.

Two-photon absorption by the host matrix and subsequent reduction by the photoexcited host present an alternative and perhaps more likely pathway for the photogeneration of silver particles. All different matrixes investigated absorb in the spectral region corresponding to the absorption of two visible photons of the wavelengths utilized for the nanoparticle generation. Such a mechanism would be related to recent work by Saponjic et al., who demonstrated photoreduction of silver and copper ions on surface-modified nanocrystalline titanium dioxide films.[45,46] Instead of multiphoton excitation using visible light sources, a UV light source in these studies was employed to excite an electron−hole pair in the $TiO_2$ support. Silver or copper ions present on the modified surface of the semiconductor nanoparticle could be reduced by rapid electron capture prior to electron−hole pair recombination. Yablonovitch and coworkers demonstrate near-infrared two-photon photogeneration of silver nanoparticles on photographic film and in a dielectric silica gel matrix.[29,30] In a related effort, Stellacci et al. show photoreduction of silver ions by a two-photon absorption process in a nanocomposite material containing among other components a silver salt and an efficient two-photon dye absorbing at 800 nm.[31] Interestingly, this dye acts as a photosensitizer both in the visible and by two-photon absorption in the near-infrared, providing a reducing agent generated optically in the focus of a laser beam. In both reduction mechanisms discussed above, nucleation is followed by continued photoreduction and aggregation, facilitated by the high concentration of silver ions in the film and a strong thermodynamical driving force for the formation of larger silver clusters.[47,48]

It is worth noting that such two-photon-based generation of luminescent nanoparticles offers novel prospects for optical storage material. Information may be stored using wavelengths in the green and blue parts of the electromagnetic spectrum, while nondestructive reading may be achieved by using red light sources. The storage capacity is in principle only limited by the diffraction-limited spot size, with full three-dimensional reading/writing achieved by lateral translation and adjusting the focal plane. Indeed, the nonlinear dependence on illumination power makes such an application particularly attractive, as this would further increase spatial resolution along the optical axis.

**IV.2. Silver Particle Distribution.** Information on the sizes of the photogenerated silver particles may be obtained by comparing the absorption spectrum in Figure 3 to a simulation of the surface plasmon resonance. This band is exquisitely sensitive to the shape and size of a noble metal particle as well as the electromagnetic properties of its environment. In the case of Ag, it may be tuned from its vacuum position (350 nm) throughout the visible and near-infrared well into the mid-infrared part of the electromagnetic spectrum.[6,7,49−51] Furthermore, when the distance between individual particles is comparable to the particle size, plasmons of individual particles interact and form cluster surface plasmon modes,[52,53] thereby significantly altering the optical properties with respect to the individual particle. Simulation of the particle size distribution is greatly simplified by assuming the silver particles to be spherical, completely embedded in the polystyrene matrix, and widely spaced with respect to their radius. In this case, the absorption cross-section of the spherical silver particles can be calculated on the basis of Mie theory.[6] At very small particle sizes, Mie theory must be extended to account for the mean free path limitation of the free conduction electrons upon scattering at the particle boundaries. This modifies the complex part of the silver dielectric function $\epsilon = \epsilon' + i\epsilon''$ to[50]

$$\epsilon''(\omega,r) = \epsilon''_{\text{bulk}} + \frac{3\omega_p{}^2 v_F}{4\omega^3 r}$$

Here we have the angular frequency $\omega$, the plasma frequency $\omega_p = 1.38 \times 10^{16}\ s^{-1}$ (see ref 50), and the Fermi velocity of the silver conduction electrons $v_F = 1.39 \times 10^6$ m/s.[55] The mean free path limitation leads to an increased plasmon bandwidth with decreasing size of the particle.

The photogeneration mechanism will give rise to a distribution of particles of different sizes in the sample. Some indication of the size distribution may be obtained by calculating absorption spectra for three different radii (1, 5, and 20 nm), whose plasmon frequencies capture the width of frequencies observed. Superpositions of these spectra are then used to least-squares fit the experimental spectrum in Figure 3, and thereby estimate the contribution of each size. For such a fit, the relative contributions by volume are 72.2(16)%, 14.03(72)%, and 13.76(53)% for particles with radii of 1, 5, and 20 nm, respectively. The inset in Figure 3 shows this size distribution. Notice that this results in a particle distribution completely dominated by the smallest particles used in the simulation, i.e., particles with a radius of 1 nm. The resulting absorption spectrum is shown as the dashed curve in Figure 3, in reasonable agreement with the principal feature of the experimental absorption spectrum. The large width of this feature requires the presence of many small particles, while the absorption maximum at 432 nm requires a contribution from larger particles. Since the absorption cross-section scales with the particle volume, we expect the majority of particles present in the sample to be small (in our simulation with a 1 nm radius), with minute concentrations of larger particles (in our case with 5 and 20 nm radii). This is consistent with a photoactivation process, where prevalence of small particles may be expected, each generated from an individual nucleation center. The growth of large particles is expected to be much slower, limited by the agglomeration rate for small particles.

The extracted distribution is based on a number of approximations. We have assumed the particles to be spherical, of three ad hoc sizes, and widely spatially separated. The constituent spectra for the spectral simulation have considerable overlap; the fitting parameters, i.e., the relative contributions of each particle size, are therefore correlated. Finally, it is important to mention that the injection of holes into metallic silver nanoparticles broadens and red shifts the plasmon band.[56] Such a situation might arise with excess silver ions adhering to the particle. Thus, the distribution shown in Figure 3 constitutes an upper limit to the sizes present in the diffraction-limited spot. While these assumptions only allow qualitative conclusions on the size distribution of the photogenerated silver nanoparticles, the main result from the simulations remains: The absorption spectrum shows a distribution or agglomerate dominated by relatively small particles. To the extent that the particles giving rise to the absorption spectrum and the particles generated in the microscope focus are comparable, the main contribution consists of nanoparticles with radii on the order of a few nanometers.

**IV.3. SERS-Active Species.** In this section we discuss the chemical nature of the Raman scattering entity. The spectra observed in our experiments extend for more than 5000 $cm^{-1}$ at all excitation wavelengths. Above 2000 $cm^{-1}$, the spectra show only a very broad and diffuse structure fluctuating in

synchrony with the strongest feature of the spectra (see, e.g., the high-frequency shift tail in the spectra in Figure 5). There is ample evidence of a broad, fluctuating continuum in SERS spectra.[22,57,58] This background is not easily explained by excitation of molecular Raman transitions. Brus and co-workers argued that the origin of this continuum lies in impurity sites on the silver particle,[59] thereby relaxing the momentum conservation rules prohibiting direct electronic Raman scattering from silver particles.[60−62] A different interpretation is given by Burstein et al.,[63] who interpret the continuum part of the Raman spectrum as originating from metal luminescence. In light of recent reports on enhanced fluorescence from noble metal nanoparticles[12] and rough metal surfaces,[11] this is a particularly intriguing suggestion. However, the spectral features in this region are sufficiently diffuse to preclude further analysis at this point.

Some information about the likely adsorbate molecules can be obtained from the most prominent feature in the Raman spectra of Figure 6, the collection of bands between 800 and 1800 $cm^{-1}$. Most SERS work is plagued by strong Raman transitions appearing in the exact range of 800−1800 $cm^{-1}$, often attributed to impurities or so-called "carbonaceous contaminations".[64−66] Establishing the nature of these impurities has however proved to pose a formidable challenge. Tsang and co-workers attributed broad Raman bands ($\Gamma_{fwhm} > 200$ $cm^{-1}$) at 1350 and 1550 $cm^{-1}$, observed from a variety of silver substrate film samples, to amorphous graphite-like carbon.[67] Remarkably, these authors claimed to observe graphitic bands even under ultra-high-vacuum conditions on a sputter-cleaned silver surface at less than a tenth of a monolayer carbon coverage as determined by atomic emission spectroscopy (AES). A number of studies indicate an important role of wavelength-dependent photodecomposition processes enhanced by the surface,[58] forming the strongly Raman-active graphite-like carbon with Raman cross-sections approximately 2 orders of magnitude larger than those of diamond.[68] Pemberton et al. showed that exposure of a variety of polycrystalline silver surfaces to the ambient $O_2$ levels produces strong, broad bands in the same frequency range.[65] Of particular relevance is a detailed investigation by Kudelski and Pettinger[69] on Raman bands from carbon chains on silver and gold films. Using a Raman microscope equipped with high-numerical-aperture objectives, they observed Raman spectra on all substrates, displaying a broad feature in the region of 800−1700 $cm^{-1}$ with a *random, fluctuating* substructure. Interestingly, when they averaged over either 40 spectra or an area considerably larger than the several square micrometers in the focal spot of their microscope, the spectra showed the two bands at approximately 1350 and 1550 $cm^{-1}$ generally attributed to carbonaceous contaminations. The fluctuating spectra were only observed in the presence of oxygen and could not be detected in coadsorbed pyridine, ruling out oxygen-induced dynamical changes to the noble metal surfaces; instead, the observations were interpreted as chemical changes to the carbon chains in the presence of oxygen. Spectral jumps may also arise from formation and breakage of weak chemical bonds between the adsorbate and the metal particle surface in room-temperature samples. Similarly, adsorbate molecules have enough energy available to rotate around metal−adsorbate bonds and may thus experience locally varying electric field enhancements. A contribution of such thermal processes to the fluctuating luminescence rates and spectra observed in our experiments seems plausible, provided the number of scatterers in the focal volume is small. In fact, several research groups attributed the widely observed spectral fluctuations in single-molecule SERS data to thermally assisted diffusion of either adsorbate molecules[59,69−71] or silver atoms along the silver metal structure.[71]

Despite the frequent observation of "carbonaceous" Raman bands in SERS, the origin and abundance of graphite-like Raman bands are still unclear. However, the spectral region and dynamical behavior of the strongest Raman bands in Figure 5 are suggestive of a connection in particular to Kudelski and Pettinger's observations on carbon chains adsorbed on noble metal surfaces.[69] This raises the possibility that a carbon-containing impurity at very low concentration, possibly photo-produced, may turn into a dominant feature in the spectra, perhaps via a resonance-enhanced Raman scattering process. Although the silver ions are embedded in a polymer matrix, the spectra are qualitatively similar in shape and strength if the sample is prepared by spin-casting a silver salt solution without the polymer directly onto the glass surface. Thus, the polymer matrix is not likely to be responsible for the SERS bands in the region of 800−1800 $cm^{-1}$. Furthermore, these bands are observed for both the silver perchlorate in toluene and the silver nitrate in chloroform and ethanol solutions, thereby eliminating any solvent-specific or counterion contribution. Notice also that our data are not consistent with the observation of counterion Raman bands as reported by Sanchéz-Cortés et al.;[66] no persistent spectral features are present in any of the recorded spectra in either $AgClO_4$ or $AgNO_3$ samples, beyond the existence of the very broad feature of overlapping bands between 800 and 1800 $cm^{-1}$. Our sample does not contain colloidal silver particles generated by the citrate reduction method.[72] It cannot display the so-called "anomalous" bands[66] exhibited in spectra associated with such particles and attributed to Raman transitions in the citrate counterion and the citrate−silver complex. While the spectra in Figure 5 show bands and behavior widely reported in the literature, we cannot determine the SERS-active species at present. Direct comparison of Raman spectra from a known species on photogenerated silver nanoparticles with the dominant bands in the spectra of Figure 6 will help to assess the likelihood of an impurity as the source of the graphite-like SERS bands.

Consideration should be given also to the likely particle sizes responsible for the observed Raman signal. SERS-active nanoparticles have typically a radius on the order of tens of nanometers and are often slightly aggregated.[41,57,72] On the basis of the approximate size distribution dominated by smaller nanoparticles as discussed in section IV.2, it is likely that SERS is only observed from the larger particles in our distribution or from aggregates of multiple particles.[57]

## V. Summary

We have demonstrated the ability to generate luminescent silver nanoparticles in a diffraction-limited spot, thus providing an all-optical "synthesis" route to silver particles. While a number of reports have previously described photoreduction of silver salts to form nanoparticles at a range of different wavelengths,[16,27−33] the present work describes several unusual and highly interesting properties of photogenerated silver particles in polymer matrixes. During generation and illumination intense luminescence is detected exhibiting strong intensity modulations, which may be related to surface-enhanced Raman scattering from $sp^2$-hybridized carbon centers. The distribution of silver nanoparticles is likely to contain predominantly very small particles with radii on the order of a few nanometers. The higher order intensity dependence of the photogeneration process points to a complicated photochemical cascade possibly involving a silver oxide as an intermediate. Experiments further

investigating the photochemistry and the structure of the silver nanoparticles are under way.

The small size of silver particles generated in our samples allows for a number of interesting observations. The particle size falls into the range of transition between molecule-like minute clusters and the larger metal nanoparticles with well-established, strong surface plasmon resonances. Thermodynamics favors the agglomeration of silver atoms and growth beyond the smallest cluster sizes containing only very few atoms, consistent with our observations. Strikingly, despite the small size of the particles, we observe strong Raman scattering, most likely surfaced-enhanced, though it is also possible that fluorescence from the metal particles contributes to the observed spectra. The transition from fluorescence to Raman scattering is intimately connected with the particle size and likely to be quite smooth. Considerable effort in studying particles in this small size range is needed to elucidate this transition further.

While there exist a number of synthetic electrochemical methods for the preparation of silver nanoparticles with tunable and exquisitely narrow size and shape distributions,[7,73] there are distinct advantages to a photoinduced synthesis. The ability of optical generation of stable, strongly luminescent silver nanoparticles[15,16,33] has potential for diffraction-limited, three-dimensional data storage[30,31] using a simple microscope setup and visible light sources. We are currently working toward utilizing these photogenerated silver particles as potentially ultrasensitive Raman sensors of trace analyte species, with ultimate prospects for detection limits down at the single-molecule level.[24]

**Acknowledgment.** We are indebted to K. L. Rowlen and P. C. Andersen for valuable discussions. Support for this work has been provided by the Air Force Office of Scientific Research (D.J.N.) and the National Science Foundation (D.J.N. and J.T.F.). O.L.A.M. gratefully acknowledges the Swiss National Science Foundation for a postdoctoral fellowship. J.T.F. is a Dreyfus Teacher-Scholar and a Research Corporation Cottrell Scholar, and thanks the JILA Visiting Fellows program for support during the period in which this research was initiated. Special gratitude is expressed to Richard Farrer for sharing the results of his experiments on two-photon photoreduction of silver salts.

**Note Added after ASAP Posting.** This article was posted ASAP on 01/08/2004. The copyright line has been changed from what was posted previously. The correct version was posted on 01/15/2004.

## References and Notes

(1) Empedocles, S. A.; Neuhauser, R.; Shimizu, K.; Bawendi, M. G. *Adv. Mater.* **1999**, *11*, 1243.
(2) Link, S.; El-Sayed, M. A. *Int. Rev. Phys. Chem.* **2000**, *19*, 409.
(3) Andersen, P. C.; Rowlen, K. L. *Appl. Spectrosc.* **2002**, *56*, 124A.
(4) Henglein, A. *Chem. Rev.* **1989**, *89*, 1861.
(5) Alivisatos, A. P. *J. Phys. Chem.* **1996**, *100*, 13226.
(6) Bohren, C. F.; Huffman, D. R. *Absorption and Scattering of Light by Small Particles*, 1st ed.; John Wiley & Sons: New York, 1983.
(7) Linnert, T.; Mulvaney, P.; Henglein, A.; Weller, H. *J. Am. Chem. Soc.* **1990**, *112*, 4657.
(8) Nicewarner-Pena, S. R.; Freeman, R. G.; Reiss, B. D.; He, L.; Pena, D. J.; Walton, I. D.; Cromer, R.; Keating, C. D.; Natan, M. J. *Science* **2001**, *294*, 137.
(9) Mooradian, A. *Phys. Rev. Lett.* **1969**, *22*, 185.
(10) Apell, P.; Monreal, R.; Lundqvist, S. *Phys. Scr.* **1988**, *38*, 174.
(11) Boyd, G. T.; Yu, Z. H.; Shen, Y. R. *Phys. Rev. B* **1986**, *33*, 7923.
(12) Mohamed, M. B.; Volkov, V.; Link, S.; El-Sayed, M. A. *Chem. Phys. Lett.* **2000**, *317*, 517.
(13) Wilcoxon, J. P.; Martin, J. E.; Parsapour, F.; Wiedenman, B.; Kelley, D. F. *J. Chem. Phys.* **1998**, *108*, 9137.
(14) Link, S.; Beeby, A.; FitzGerald, S.; El-Sayed, M. A.; Schaaff, T. G.; Whetten, R. L. *J. Phys. Chem. B* **2002**, *106*, 3410.
(15) Zheng, J.; Dickson, R. M. *J. Am. Chem. Soc.* **2002**, *124*, 13982.
(16) Peyser, L. A.; Vinson, A. E.; Bartko, A. P.; Dickson, R. M. *Science* **2001**, *291*, 103.
(17) Varnavski, O.; Ispasoiu, R. G.; Balogh, L.; Tomalia, D.; Goodson, T. *J. Chem. Phys.* **2001**, *114*, 1962.
(18) Kiely, C. J.; Fink, J.; Brust, M.; Bethell, D.; Schiffrin, D. J. *Nature* **1998**, *396*, 444.
(19) Lee, D. I.; Donkers, R. L.; DeSimone, J. M.; Murray, R. W. *J. Am. Chem. Soc.* **2003**, *125*, 1182.
(20) Kreibig, U.; Bour, G.; Hilger, A.; Gartz, M. *Phys. Status Solidi A* **1999**, *175*, 351.
(21) Jeanmaire, D. L.; Van Duyne, R. P. *J. Electroanal. Chem.* **1977**, *84*, 1.
(22) Michaels, A. M.; Jiang, J.; Brus, L. *J. Phys. Chem. B* **2000**, *104*, 11965.
(23) Gersten, J. I. *J. Chem. Phys.* **1980**, *72*, 5779.
(24) Nie, S. M.; Emory, S. R. *Science* **1997**, *275*, 1102.
(25) Otto, A.; Mrozek, I.; Grabhorn, H.; Akemann, W. *J. Phys.: Condens. Matter* **1992**, *4*, 1143.
(26) Kneipp, K.; Kneipp, H.; Itzkan, I.; Dasari, R. R.; Feld, M. S. *Chem. Rev.* **1999**, *99*, 2957.
(27) Muniz-Miranda, M. *J. Raman Spectrosc.* **2002**, *33*, 295.
(28) Crawford, K. D.; Hughes, K. D. *J. Phys. Chem. B* **1998**, *102*, 2325.
(29) Wu, P. W.; Dunn, B.; Yablonovitch, E.; Doan, V.; Schwartz, B. J. *J. Opt. Soc. Am. B* **1999**, *16*, 605.
(30) Wu, P. W.; Cheng, W.; Martini, I. B.; Dunn, B.; Schwartz, B. J.; Yablonovitch, E. *Adv. Mater.* **2000**, *12*, 1438.
(31) Stellacci, F.; Bauer, C. A.; Meyer-Friedrichsen, T.; Wenseleers, W.; Alain, V.; Kuebler, S. M.; Pond, S. J. K.; Zhang, Y. D.; Marder, S. R.; Perry, J. W. *Adv. Mater.* **2002**, *14*, 194.
(32) Peyser, L. A.; Lee, T. H.; Dickson, R. M. *J. Phys. Chem. B* **2002**, *106*, 7725.
(33) Farrer, R. A.; Kempa, T.; Fourkas, J. T. Manuscript in preparation.
(34) Eachus, R. S.; Marchetti, A. P.; Muenter, A. A. *Annu. Rev. Phys. Chem.* **1999**, *50*, 117.
(35) Fedrigo, S.; Harbich, W.; Buttet, J. *J. Chem. Phys.* **1993**, *99*, 5712.
(36) Felix, C.; Sieber, C.; Harbich, W.; Buttet, J.; Rabin, I.; Schulze, W.; Ertl, G. *Chem. Phys. Lett.* **1999**, *313*, 105.
(37) Marchetti, A. P.; Muenter, A. A.; Baetzold, R. C.; McCleary, R. T. *J. Phys. Chem. B* **1998**, *102*, 5287.
(38) Zhang, X.; Hendro, W.; Fujii, M.; Tomimura, T.; Imaishi, N. *Int. J. Thermophys.* **2002**, *23*, 1077.
(39) Hartland, G. V.; Guillaudeu, S.; Hodak, J. H. Laser induced alloying in metal nanoparticles. In *Molecules as Components in Electronic Devices*; Liebermann, M., Ed.; ACS Symposium Series No. 844; American Chemical Society: Washington, DC, 2003.
(40) Hodak, J. H.; Henglein, A.; Giersig, M.; Hartland, G. V. *J. Phys. Chem. B* **2000**, *104*, 11708.
(41) Kneipp, K.; Wang, Y.; Kneipp, H.; Perelman, L. T.; Itzkan, I.; Dasari, R.; Feld, M. S. *Phys. Rev. Lett.* **1997**, *78*, 1667.
(42) Belloni, J. *C. R. Phys.* **2002**, *3*, 381.
(43) Varkey, A. J.; Fort, A. F. *Sol. Energy Mater. Sol. Cells* **1993**, *29*, 253.
(44) Kotz, R.; Yeager, E. *J. Electroanal. Chem.* **1980**, *111*, 105.
(45) Rajh, T.; Nedeljkovic, J. M.; Chen, L. X.; Tiede, D. M.; Thurnauer, M. C. *J. Adv. Oxide Technol.* **1998**, *3*, 292.
(46) Saponjic, Z. V.; Rajh, T.; Nedeljkovic, J. M.; Thurnauer, M. C. Photoinduced deposition of copper on nanocrystalline TiO2 films. In *Trends in Advanced Materials and Processes*; 2000; Vol. 352, p 91.
(47) Henglein, A. *Ber. Bunsen-Ges. Phys. Chem.* **1990**, *94*, 600.
(48) Henglein, A.; Mulvaney, P.; Linnert, T. *Faraday Discuss.* **1991**, 31.
(49) Gersten, J.; Nitzan, A. *J. Chem. Phys.* **1981**, *75*, 1139.
(50) Kreibig, U. *J. Phys. F: Met. Phys.* **1974**, *4*, 999.
(51) Lynch, D. W.; Hunter, W. R. Optical Constants of Metals. In *Handbook of Optical Constants of Solids*; Palik, E. D., Ed.; Academic Press: New York, 1985; p 275.
(52) Kreibig, U.; Genzel, L. *Surf. Sci.* **1985**, *156*, 678.
(53) Meier, M.; Wokaun, A.; Liao, P. F. *J. Opt. Soc. Am. B* **1985**, *2*, 931.
(54) Kreibig, U. *Z. Phys.* **1970**, *234*, 307.
(55) Ashcroft, N. W.; Mermin, N. D. *Solid State Physics*, 1st ed.; International Thomson Publishing: 1976.
(56) Kreibig, U.; Vollmer, M. *Optical Properties of Metal Clusters*; Springer-Verlag: Berlin, 1995.
(57) Michaels, A. M.; Nirmal, M.; Brus, L. E. *J. Am. Chem. Soc.* **1999**, *121*, 9932.

(58) Otto, A. *J. Raman Spectrosc.* **2002**, *33*, 593.
(59) Bosnick, K. A.; Jiang, J.; Brus, L. E. *J. Phys. Chem. B* **2002**, *106*, 8096.
(60) Portales, H.; Duval, E.; Saviot, L.; Fujii, M.; Sumitomo, M.; Hayashi, S. *Phys. Rev. B* **2001**, *6323*, 233402.
(61) Itai, K. *Phys. Rev. B* **1992**, *45*, 707.
(62) Zawadowski, A.; Cardona, M. *Phys. Rev. B* **1990**, *42*, 10732.
(63) Burstein, E.; Chen, Y. J.; Chen, C. Y.; Lundquist, S.; Tosatti, E. *Solid State Commun.* **1979**, *29*, 567.
(64) Norrod, K. L.; Rowlen, K. L. *Anal. Chem.* **1998**, *70*, 4218.
(65) Taylor, C. E.; Garvey, S. D.; Pemberton, J. E. *Anal. Chem.* **1996**, *68*, 2401.
(66) Sanchez-Cortes, S.; Garcia-Ramos, J. V. *J. Raman Spectrosc.* **1998**, *29*, 365.
(67) Tsang, J. C.; Demuth, J. E.; Sanda, P. N.; Kirtley, J. R. *Chem. Phys. Lett.* **1980**, *76*, 54.
(68) Wada, N.; Solin, S. A. *Physica B+C* **1981**, *105*, 353.
(69) Kudelski, A.; Pettinger, B. *Chem. Phys. Lett.* **2000**, *321*, 356.
(70) Moyer, P. J.; Schmidt, J.; Eng, L. M.; Meixner, A. J. *J. Am. Chem. Soc.* **2000**, *122*, 5409.
(71) Weiss, A.; Haran, G. *J. Phys. Chem. B* **2001**, *105*, 12348.
(72) Lee, P. C.; Meisel, D. *J. Phys. Chem.* **1982**, *86*, 3391.
(73) Creighton, J. A.; Blatchford, C. G.; Albrecht, M. G. *J. Chem. Soc., Faraday Trans.* **1979**, *75*, 790.